RSC Applied Polymers

ROYAL SOCIETY OF CHEMISTRY

PAPER

View Article Online
View Journal

Cite this: DOI: 10.1039/d5lp00407a

Tuning the functionality of acrylated vegetable oil: impact on the physicochemical properties of the 3D printed network

Anthony Jolly, Ana Tanase, Étienne Durand-Laberge and Audrey Laventure *

Vat photopolymerization (VP) processing, an additive manufacturing (AM) technique, relies on the photopolymerization of light-sensitive resins. However, most commercially available resins are petrosourced and non-biodegradable. Recent reports have highlighted vegetable oils (VO) as promising bio-based alternatives, although their native carbon–carbon double bonds exhibit poor reactivity in free-radical polymerization. This limitation has been overcome by introducing polymerizable groups such as acrylates. Taking into account the growing interest in VO-derived resins, developing a deeper understanding of the influence of the acrylate functionality on the formulation behavior and the resulting 3D printed material performance is critical to enable a better control over their properties. In this work, canola oil (CO), a highly available feedstock in Canada, was acrylated to obtain resins with functionalities ranging from 1.87 to 2.78 average number of acrylate groups per molecule. The resulting formulations were characterized rheologically, photochemically, and mechanically. Our results show that increasing the average acrylate functionality per CO molecule leads to a lower critical energy (E_c) and penetration depth (D_p) in the context of the resin photopolymerization. Conversely, higher functionality improved the mechanical performance of the 3D printed samples, with tensile modulus increasing from 9 MPa to 18 MPa. This work deepens our understanding of how the degree of acrylation of CO influences the properties of 3D printed materials, enabling the establishment of structure–processing–property relationships leading to a more rational design of these biobased photopolymerizable compounds.

Received 22nd December 2025,
Accepted 9th April 2026

DOI: 10.1039/d5lp00407a

rsc.li/rscapplpolym

Introduction

New technologies, such as additive manufacturing (AM), also referred to as three-dimensional (3D) printing, are emerging. This rapidly expanding processing technique offers numerous advantages, including the capability to create complex shapes and reduce waste compared to traditional manufacturing processes. Among the various AM approaches, vat photopolymerization (VP) techniques, including Stereolithography (SLA), Digital Light Processing (DLP) and Masked Stereolithography (MSLA), rely on the photopolymerization of UV-sensitive resin formulations.[1,2] This method enables the fabrication of complex parts with a resolution of ~10 μm. While recent efforts have enabled the development of biosourced resins, most of the compounds entering the commercial formulations used today are derived from petroleum and are not biodegradable.

The development of biobased monomers represents a promising alternative.[3–16] Among the various available sources, vegetable oils (VO) stand out as renewable alternatives to petroleum-based polymers, especially for VP processing as it is in liquid form. Composed of triglycerides, *i.e.* glycerol esters linked to three long chains of fatty acids whose composition varies depending on the oil source, VO offer several advantages, including biodegradability and availability, while also featuring functional groups suitable for functionalization.[17,18] Vegetable oils contain multiple carbon–carbon double bonds. However, these bonds exhibit low reactivity for free radical polymerization. The introduction of polymerizable groups, such as acrylate, is the most convenient way to overcome this obstacle. Such functional groups are most conveniently introduced through reacting epoxidized oil with acrylic acid.[14,19–24] Nevertheless, a one-step reaction was introduced by the Zhang group, avoiding the epoxidation of the double bonds, reducing the number of steps, thus saving energy.[25]

These advances enable the transformation of vegetable oils into monomers for VP 3D printing resins. This approach represents an innovative and sustainable approach, paving the way for more environmentally friendly polymer materials. Several studies have demonstrated the effectiveness of vegetable oils in this field, especially using soybean oil.[26–31] The

Département de chimie, Université de Montréal, 1375 Ave. Thérèse-Lavoie-Roux, Montréal, QC, Canada H2V 0B3. E-mail: audrey.laventure@umontreal.ca

Blasco group has also compared different vegetable oil sources (sunflower, canola, soybean, olive, and sesame oil) and investigated their physicochemical properties for AM, expanding the library of possible vegetable oil to exploit.[32] Other studies have also explored the potential of using waste oils for 3D printing as a primary source, avoiding the use of commercial food resources and decreasing the amount of waste generated.[33,34] Their biodegradability was also measured in soil burial tests over 14 days leading to a large weight loss (~25%) compared to ~2% for a commercial resin.[34]

However, the impact of the variation of the average number of functional groups per VO molecule on the physicochemical properties of the formulations and the resulting 3D printed samples has not been studied yet. This gap in knowledge is important to address as understanding these relationships leads to a better control to tune the properties of the resins and the resulting 3D printed samples. In this work, the impact of the systematic modulation of the average number of acrylates per molecule on the physicochemical properties of acrylated canola oil (ACO) and resulting 3D prints were studied. First, canola oil (CO), selected for its abundance in Canada, was functionalized to obtain acrylation levels ranging from an average number between 1.87 and 2.78 acrylate groups per CO molecule. The compounds were formulated into a photoreactive resin that was characterized by optical and rheological analyses. Their curing behavior, as well as the thermal and mechanical properties of the resulting 3D printed samples were compared. This study deepens our understanding of how the degree of acrylation influences the physicochemical properties of the CO molecules, thus leading to quantitative structure-processing-property relationships that can be leveraged into rational design and formulation guidelines for the development of bio-derived photopolymerizable resins.

Experimental section

Material

Boron trifluoride diethyl etherate (BF_3Et_2O) was obtained from Millipore-Sigma. Acrylic acid (low water content, 99.5%, stab. with *ca.* 200 ppm 4-methoxyphenol) and hexane were obtained from Thermo Fisher Scientific. Canola oil was purchased in a grocery store (Montréal, Canada). Bis(2,4,6-trimethylbenzoyl)-phenylphosphineoxide (BAPO) and $MgSO_4$ were purchased from A2B Chem. $NaHCO_3$ and NaCl were obtained from ACP chemicals. Chloroform-*d* ($CDCl_3$, 99.8 atoms % D) was purchased from Millipore-Sigma utilized as a solvent for NMR measurements.

Synthesis of the acrylated oil

In a 500 mL two neck round bottom flask, canola oil (100 g, 1 equiv.), (1 equiv. = 1 molar equivalent) acrylic acid (62 to 246 mL, 8 to 32 equiv.) and 4-methoxyphenol (46 mg) were mixed at room temperature for 5 min. Boron trifluoride diethyl etherate BF_3OEt_2 (10.4 mL, 0.7 equiv.) was slowly added to the reaction mixture at room temperature. The reaction was protected from light with aluminium foil to avoid polymerization and was then heated at 80 °C for 18 h. Once cooled, hexane (200 mL) was added, and the mixture was washed with 5% aqueous $NaHCO_3$ solution until no more gas was formed during shaking (warning: it produces a lot of pressure when shaken in a separating funnel). The organic phase was washed with brine, dried over $MgSO_4$ and the solvent was evaporated under. The product obtained was an orange oil.

^{1}H NMR (400 MHz, $CDCl_3$): δ (ppm) = 6.42 (m, H_a), 6.14 (m, H_b), 5.86 (m, H_c), 5.35 (m, H_d/H_e), 4.96 (m, H_f), 4.31 (m, H_g), 2.72 (m, H_h), 2.33 (m, H_i), 1.99 (m, H_j), 1.99 (m), 1.59 (m), 1.28 (m), 0.99 (t, J = 12 Hz).

Formulations for MSLA

MSLA formulations were prepared by mechanically mixing the acrylated oil with BAPO (2 wt%). The blend was mixed for at least 1 h at around 200 rpm. It was protected from light with aluminium foil to avoid undesired polymerization.

Characterization

Nuclear magnetic resonance (NMR). ^{1}H NMR measurements were recorded on a Bruker AV400 MHz spectrometer in $CDCl_3$ unless stated otherwise, using solvent peaks as internal standards ($CHCl_3$: δ: 7.26 ppm).

Fourier transform infrared spectroscopy (FTIR). The Fourier transform infrared (FT-IR) spectra with wavelength from 4000 to 600 cm^{-1} were recorded by a Nicolet 4700 spectrophotometer using an attenuated total attenuation (ATR) accessory equipped with a diamond crystal, and a resolution of 2 cm^{-1} for 32 background and sample scans.

UV-Vis spectroscopy. UV-Vis spectroscopy (Agilent Technologies Cary 60 UV-Vis) was used to investigate the absorption profile of the different oils. The latter were dissolved in chloroform at a concentration of 5.7 mM and the absorbance was measured in a quartz cell between 300–800 nm.

Rheology. Rheological analyses were performed using an Haake MARS 60 (Thermo Scientific Instruments) rheometer. A plate–plate (PP) geometry with a diameter of 20 mm and a 0.75 mm gap was used. Viscosity was measured as a function of a shear rate ranging from 0.1 to 90 s^{-1} under isothermal conditions (25 °C).

Masked SLA (MSLA). 3D printing was carried out by using a Prusa SL1S printer with a 405 nm LED light source. The pixel resolution of the 3D printer is 2560 × 1620p. The prints were performed at room temperature with a layer thickness of 50 μm. The exposure time and intensity were set to 20 s and 1.2 mW cm^{-2}, respectively. After printing, the excess resin was drained from the parts and platform to be reused. The building platform was taken out of the printer, and the parts were removed carefully using a blade. The printed parts were then washed and sonicated with hexane. Thereafter, the objects were cured in a Prusa CW1S UV chamber for 30 min. Finally, the parts were stored protected from light.

Cure depth measurements. Freshly prepared formulation was deposited inside a homemade apparatus (Fig. S1). This apparatus was deposed onto the screen of the MSLA printer

and exposed to UV light (405 nm) for different time. Light intensity was found to be 1.2 mW cm^{-2}, on the surface area where the device was deposed. After the exposition, uncured ink was intensively rinsed with hexane. The sample was cured for 1 min in the UV chamber, and its dimensions were measured using a digital calliper Mitutoyo MDC-1″SXF with a 0.001 mm precision.

Thermogravimetric analyses (TGA). TGA were performed using a Discovery TGA 5500 device (TA Instruments). Samples were placed in an aluminium pan. The analyses were conducted over a temperature range of 25 °C to 600 °C at a heating rate of 10 °C min^{-1}, with a nitrogen flow of 100 mL min^{-1}.

Differential scanning calorimetry analyses (DSC). DSC were performed using a DSC 2500 (TA Instruments). Samples were placed in a hermetic aluminium pan. The thermal behaviour of the samples was investigated by using two repeated heating–cooling cycles between −60 °C and 100 °C at a heating and cooling rate of 10 °C min^{-1} using a nitrogen atmosphere and indium for calibration. The glass transition temperature (T_g) was determined from the second heating curve.

Mechanical analyses. Tensile tests were performed at room temperature on an Instron 5565 testing machine with a 500 N static load cell and a crosshead speed of 1.00 mm min^{-1}. Type 1BB tensile test specimens were printed with a layer thickness of 50 μm. Five specimens of each material were tested and analysed.

Results and discussion

Synthesis and characterization

Vegetable oils consist of a distribution of triglycerides, glycerol esters linked to three long fatty acid chains. The composition of these chains varies depending on the oil source, resulting in a mixture of different molecular structures. Consequently, the number of available carbon–carbon double bonds can differ from one batch to another, making the characterization of starting materials essential. Fig. 1 shows the canola oil (CO) and acrylated canola oil (ACO) molecular structures. ^{1}H NMR was used to confirm the obtention of the product, along with the proton identification. Proton H_i, which is linked to the carbonyl group in the fatty acid exhibits a distinct chemical shift (2.33 ppm) from other protons after the reaction. Due to its stability, this peak was chosen as the internal standard. The triglyceride form was confirmed by integrating protons H_i and H_g, which gave a ratio of 3 : 2. Eqn (1) was used to calculate the amount of unsaturation in CO molecules, which was found to be 3.82. This number of unsaturation is in accordance with literature where values are ranging from 3.8 to 3.9 for canola oil.[29,32]

$$\text{Double bond per oil molecule} = \left(\frac{[A_{d,e} - (A_g/4)]/2}{\left(\frac{A_i}{6}\right)} \right) \quad (1)$$

where A is the integrated area of the corresponding peaks.

Having determined the average number of double bonds in the CO molecule, the procedure reported by Zhang *et al.* was followed, employing acrylic acid and boron trifluoride diethyl etherate as a catalyst to incorporate acrylate functionalities on the CO double bonds.[25] Despite taking precautions such as working in dark conditions, self-polymerization of the acrylic acid was occasionally encountered. To address this issue, a tiny quantity of an inhibitor, 4-methoxyphenol, was included, successfully preventing further reactions. It is also important to note that BF_3OEt_2 should be added at room temperature, not at 80 °C, as it will cause immediate polymerization of acrylic acid.

To increase the number of acrylic functionalities per CO molecule, the amount of catalyst BF_3OEt_2 was varied. Originally using 0.7 equiv., 2 and 4 equiv. were also tested. Unfortunately, the use of higher proportions of BF_3OEt_2 promoted side reactions such as the transesterification of fatty acid chains with acrylic acid. Transesterification was detected on ^{1}H NMR in the region of 4 to 4.5 ppm where a shift of the proton H_g peaks was observed (Fig. 2). On the other hand, reducing the catalyst quantity from 0.7 to 0.35 equiv. led to a decrease in both transesterification and average functionality. Other groups have reported similar observation with changes in temperature.[25] When the temperature increased, the amount of transesterification increased as well. To achieve a good balance between functionality and side reactions, the catalyst was set at 0.7 equiv. Afterward, acrylic acid was added

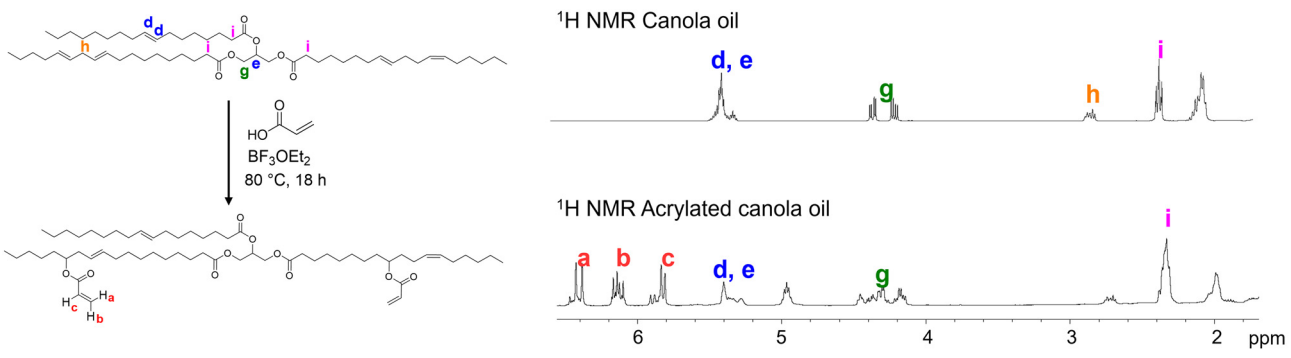

Fig. 1 Molecular structures and ^{1}H NMR of canola oil (CO) and acrylated canola oil (ACO).

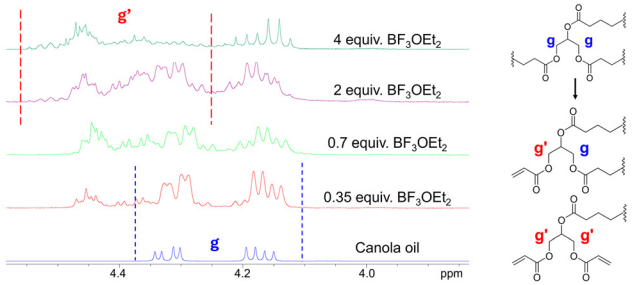

Fig. 2 Examples of transesterification side reaction.

in different quantities, specifically 8, 12, 16, 24, and 32 equiv. relative to the CO molecule. The average acrylate functional group for each reaction was determined using eqn (2) where A is the integrated area of the corresponding peaks.

$$\text{Average acrylate functionality}, \bar{f} = \frac{A_a}{A_i/6} \quad (2)$$

where $\bar{f}$ is the average functionality, A_a and A_i are the integrated areas of peaks a and i, respectively.

Fig. 3 shows how increasing the amount of acrylic acid influences the average functionality $\bar{f}$, and the reaction conversion. Increasing the amount of acrylic acid increases the average functionality, but only up to a certain plateau. The average functionality corresponds to 1.87 for 8 acrylic acid equiv., up to 2.78 for 32 equiv., resulting in an average double bond conversion of 49 to 73% respectively. These results are also shown in Table 1.

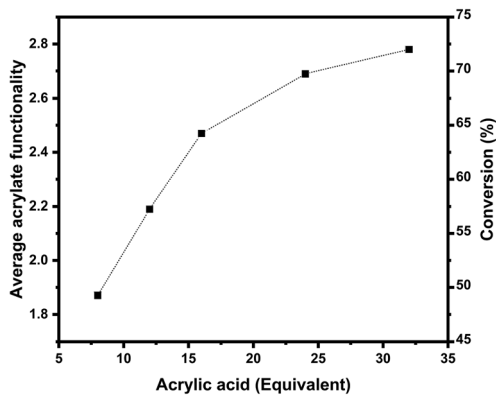

Fig. 3 Average number of acrylate functionality and corresponding conversion as a function of the quantity of acrylic acid used.

The reaction was also carried out three times using the same amount of acrylic acid (16 equiv.) and yielded the same result each time, demonstrating excellent reproducibility. Increasing the amount of acrylic acid did not affect the extent of transesterification, as evidence by unchanged ^{1}H NMR spectra in the 4.0–4.5 ppm range (Fig. S2). However, it should be noted that a variation of the functionality was observed with a different reaction scale. The functionality decreased on a smaller scale compared to a larger one (Fig. S3). We recognize that the reaction scale effects are typically observed in the opposite direction. Therefore, further investigation is required to elucidate this unexpected trend, especially regarding its implications for potential industrial-scale implementation, where a particular attention to agitation speed, impeller type, liquid level, and flask size should be made.

Characterization of the acrylated canola oil (ACO) formulations

FTIR analyses. The characterization of the ACO resin was also performed through FTIR analysis. Fig. S4A shows the ACO spectra before and after the UV irradiation. On ACO, the bands at 1722 cm^{-1} and 1193 cm^{-1} are assigned to the C=O and C–O vibration in triglycerides, respectively. The vibrations of C=C in acrylate groups are observed at 1636 and 1619 cm^{-1} and the band at 809 cm^{-1} was attributed to the *cis*-CH=CH group vibrations. The absorbance of the latter was used to follow the polymerization conversion values (Fig. S4). In every case, conversions were not complete and are ranging from 73 to 82%.

Optical analyses. The ACO compounds exhibited slightly different colorations between themselves. ACO1 and ACO2 with a $\bar{f}$ = 1.87 and 2.19, respectively appeared lighter than the remaining three, *i.e.* ACO3, ACO4 and ACO5. This visual analysis was confirmed using optical characterization. The ACO samples were therefore analysed by UV-Vis spectroscopy by diluting them in chloroform (Fig. S5), without any photoinitiator. Thus, these absorbance spectra only correspond to the ACO compounds and are not fully representative of the absorbance of the formulations used to conduct the Jacobs working curves (*vide infra*). A shoulder around 375 nm appears for the darkest specimens (ACO3, ACO4 and ACO5). Additionally, there was a decrease in the absorbance for ACO3, ACO4 and ACO5 (7.27×10^{-2}, 6.79×10^{-2}, 6.27×10^{-2}, respectively) at 405 nm as it can be seen on

Table 1 Physicochemical properties of ACO1–ACO5

Entry	Acrylic acid (equivalent)	Average acrylate functionality	Average double bond conversion (%)	Rheology Viscosity at ~30 s^{-1} (Pa s)	Curing behavior			Tensile modulus (MPa)
					E_c (mJ cm^{-2})	D_p (mm)	R^2	
ACO1	8	1.87	49	0.9	7.03	0.175	0.999	9 ± 1
ACO2	12	2.19	57	1.1	5.15	0.174	0.995	11 ± 2
ACO3	16	2.47	65	1.0	7.94	0.180	0.998	13 ± 1
ACO4	24	2.69	70	0.9	5.54	0.159	0.983	17 ± 1
ACO5	32	2.78	73	0.8	4.60	0.142	0.990	18 ± 1

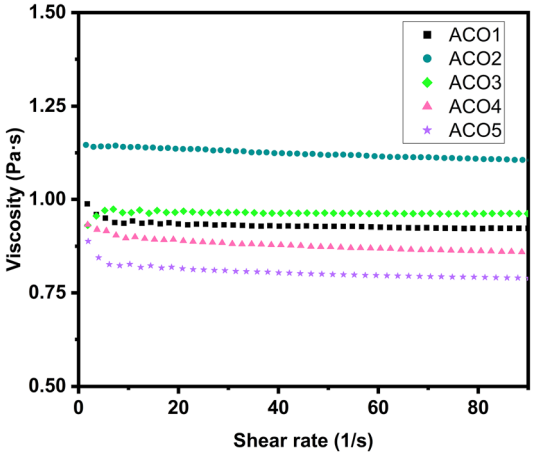

Fig. 4 Rheology analysis of ACO1–5: viscosity measured as a function of a shear rate ranging from 0.1 to 90 s^{-1} under isothermal conditions (25 °C).

the spectra. ACO1 and ACO2 compounds do not have this characteristic shoulder at 375 nm and have almost the same absorbance (4.87×10^{-2} and 4.81×10^{-2}, respectively) at 405 nm. The disparity between the two groups, ACO1–2 and ACO3–5, may be attributed to scattering effects – yet this is a hypothesis that should be studied in depth in a different study.

Rheology. The viscosity of the printing material significantly influences the 3D printing process.[35] In VP processing, the higher the viscosity, the longer the waiting time of the recoating process, and the longer the printing time. It can also cause jamming issues and may require special modifications to the printer or process to ensure optimal print quality.[36,37] In the case of vat polymerization printing, the targeted viscosity range is often between 0.2 and 10 Pa s at the shear rate of 0.1–100 s^{-1}.[38–40] Thus, to evaluate the suitability of the functionalized vegetable oils and to study the impact of the functionality on viscosity, a rotational viscometer was employed to measure their viscosity as shown in Fig. 4 and Table 1. Viscosity was measured as a function of a shear rate ranging from 0.1 to 90 s^{-1} at 25 °C and values were reported on Table 1. The viscosity of various specimens stays relatively constant, ranging between 0.8 and 1.1 ± 0.2 Pa s at ~30 s^{-1}. For ACO2–5, a slight decrease in viscosity appears to occur as functionality increases. The viscosity range is in accordance with literature.[32,41] Interestingly, all ACO demonstrate a viscosity suitable for MSLA printing, showing a minor reduction as the shear rate rises. This pattern suggests weak shears-thinning/near-Newtonian fluid behavior.

3D printing using MSLA

One of the key parameters in the determination of the printing conditions is the minimum cure energy (E_c), which is the critical exposure energy required to cure the monomer resin to its gel point. Another important aspect is the depth of penetration (D_p), which represents the distance UV light can travel into the resin before its irradiance decreases to $1/e$ (about 37%) of its initial value. If the D_p is too low compared to the desired thickness of the layers during subsequent VP printing, the bonds between the layers may not form properly. On the contrary, if the D_p is too high, the resolution can be affected.[42] The fundamental model for describing the curing behavior in a VP system is given by Jacobs equation (3), also known as the working curve, based on the Beer–Lambert law, where C_d represents the depth of the cure at a given exposure E.

$$C_d = D_p \ln\left(\frac{E}{E_c}\right) \quad (3)$$

The thickness of the polymer (single layer exposure depth (C_d)) obtained *vs.* the exposure energy (E) was plotted on a semilogarithmic graph producing a linear dependence with a slope of D_p and an x-intercept of E_c (Fig. 5). These values are also listed in Table 1. Each data point was measured in triplicate, and the average value was reported in the graph. The R^2 values of the Jacobs working curves (ranging from 0.983 to 0.999) show an excellent fit of the linear model.

Values suggest the presence of two different groups, ACO1–2 and ACO3–5, as seen in the UV-Vis analysis. Within the first group, AC01 and ACO2 have similar D_p, 0.175 mm and 0.174 mm respectively. This might be due to the fact that they have similar absorption values. However, for the second group, *i.e.*, for ACO3–5 the absorption was previously shown to decrease with increasing functionality; similarly, D_p also decreases as functionality increases, demonstrating a simultaneous decline in both values. Nevertheless, D_p cannot be directly related to the absorption, since ACO2 and ACO3 have similar D_p, but different absorption. In both groups, E_c decreases from 7.03 mJ cm^{-2} to 5.15 mJ cm^{-2} for ACO1–2 and from 7.94 mJ cm^{-2} to 4.60 mJ cm^{-2} for ACO3–5 as functionality decreases. A high average number of acrylate functionalities has a higher percentage of available acrylic groups and therefore requires lower UV intensity and exposure time to photocure. These observations are consistent with the findings of Xu

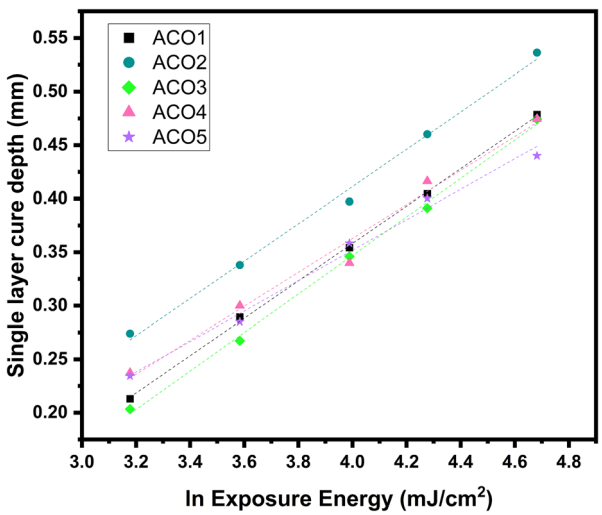

Fig. 5 Jacobs working curves for ACO1–5. E_c and D_p were extracted as x-intercept and slope, respectively.

et al., who reported that increasing the acrylate functionality of gelatin resulted in a reduction of D_p from 1.9 mm to 0.61 mm in their system.[43] The D_p values of our study, ranging between 0.142 mm to 0.180 mm, are relatively close to the desired ones, considering that the layer thicknesses during subsequent MSLA printing are between 50 and 100 μm.

Mechanical and thermal characterization

To assess how varying acrylate functionality affects the mechanical properties, tensile tests were conducted on five samples of type 1BB tensile test specimens printed from each ACO formulations (Fig. 6a). The tensile modulus was derived from the stress–strain curve's slope and displayed in Fig. 6b as a function of the average number of acrylate functionalities. As this average number rises, the tensile modulus doubles from about 9 MPa to 18 MPa, which can be attributed to an increase in the cross-linking rate. Our material shows a tensile modulus of 13 ± 1 MPa for an average number of acrylate functionalities of 2.57. This result is in line with the literature, which reports a tensile modulus of 13 ± 0.42 MPa for the same acrylate functionality for CO.[32] The elongation at break and tensile strength of all the specimens are reported in Table S1. Elongations at break are relatively close varying between 3.1 and 4.6% and have no correlation with the average functionality. Ultimate tensile strength slightly increases from 0.26 to 0.52 MPa and could be linked to the increase in the average double bond conversion. Other researchers have noticed similar outcomes in terms of tensile modulus and strain for vegetable oil-based polymers.[23,32] The tensile modulus more than doubles when the average functionality increase; nonetheless, this rise is relatively small. In comparison, a commercial resin (Anycubic Standard Resin) has a tensile modulus, tensile strength and elongation at break of around 1700 MPa, 45 MPa and 14%, respectively, which is much higher than the ones obtained with our ACOs.

However, to significantly boost the tensile modulus and optimize the elongation at break, alternative strategies, such as incorporating different monomers to form copolymers, should be explored. Several examples are found in the literature where this strategy was used, such as the group of Ostrauskaite, who mixed soybean oil and vanillin-based acrylate.[10,30,44] In some cases, the tensile modulus even surpassed GPa such as polymers made from biobased carboxylic acids with tensile modulus reaching around 4.5 GPa.[45]

Thermal analyses of ACO1–5 (Fig. S6) showed that the degradation temperature at 5% of weight loss was found to be around 243 °C ± 10 °C. The degradation temperature for each ACO is reported on Table S2. DSC analyses of ACO1–5 (Fig. S7) showed glass transition temperatures ranging from −9 to −1 °C. The exact values are reported in Table S3. Those values

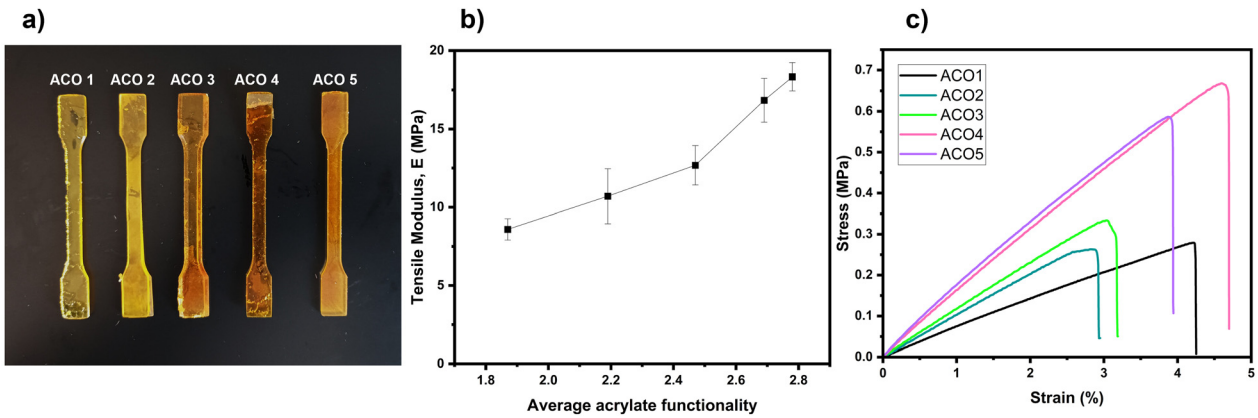

Fig. 6 Mechanical test for the different functionality. (a) 3D printed type 1BB tensile test specimens. (b) Tensile modulus as a function of the average acrylate functionality. (c) Representative stress *vs.* strain curves for ACO1–5.

Fig. 7 3D printing of (a) Lab Laventure logo, (b) and (c) Hogwarts castle.

are in the same range as different articles in literature for similar compounds.[34,44]

3D printing tests. Several prints were realized (Fig. 7) using ACO3 as it represents the midpoint formulation among the five tested resins and therefore reflects the average material performance. It should be noted that all the compounds ACO1–ACO5 were printable using MSLA as the tensile test specimens were 3D printed. All 3D structures were printed using a layer thickness of 50 μm. The exposure time was set to 90 s for the bottom layer and 20 s for others. The logo of our lab (Fig. 7a) was printed using supports that left some hole at the back of the printing. Nevertheless, the 3D print showed good overall quality. Another printing, the well-known Harry Potter™ castle (Fig. 7b and c), was realized at a relatively small scale (X 25 × Y 35 × Z 17 mm). The object demonstrated a high printing fidelity (>98%), as calculated based on the magnified views in Fig. S8. However, some fine structures, such as the bridge pillars, collapsed during the washing step, likely due to insufficient rigidity of the material.

Conclusions

In summary, we investigated how changes in the average functional group content of VO affect both the formulation properties and the performance of the 3D printed materials. CO was functionalized with different amounts of acrylic acid. All ACO formulations were printable with an excellent printing fidelity and exhibited suitable viscosities for MSLA. These results further confirm that vegetable oils are a promising alternative to petroleum-based resins. However, their mechanical performance remains lower than that of commercial petroleum-based resins, highlighting the need for complementary strategies such as co-monomer incorporation, post-curing optimization, or crosslink density enhancement. Blending ACO with other bio-based monomers would represent a promising strategy to achieve additional changes in the final material properties and unlock new classes of sustainable materials, including shape-memory polymers, advanced coatings, and next-generation additive-manufacturing resins.[41,46–48]

Conflicts of interest

There are no conflicts to declare.

Data availability

Data supporting this article have been included as part of the submitted manuscript and the supplementary information (SI). Supplementary information: ^{1}H NMR, thermal analyses and additional experimental details. See DOI: https://doi.org/10.1039/d5lp00407a.

Acknowledgements

ÉDL thanks the Natural Sciences and Engineering Research Council of Canada (NSERC) for an undergraduate student research award (USRA). AL acknowledges the Canada Research Chair program (CRC), the NSERC and the Canada Foundation for Innovation (CFI). We thank Jean-François Myre from the mechanical workshop who designed the apparatus used in the Jacobs curves analyses.

References

1 S. C. Gauci, A. Vranic, E. Blasco, S. Brase, M. Wegener and C. Barner-Kowollik, *Adv. Mater.*, 2024, **36**, e2306468.
2 S. C. Ligon, R. Liska, J. Stampfl, M. Gurr and R. Mülhaupt, *Chem. Rev.*, 2017, **117**, 10212–10290.
3 C. Bösche, L. Hagenlocher, E. Bianchi, N. Bragato, N. Lotti and T. Robert, *ACS Sustainable Chem. Eng.*, 2025, **13**, 19405–19415.
4 M. Caliari, J. Teotonico, M. Irigoyen, A. Mujika, T. Isolabella, D. Mantione, L. Irusta, B. Grignard, F. Vidal, C. Detrembleur and H. Sardon, *J. Am. Chem. Soc.*, 2025, **147**, 30095–30106.
5 P. S. Klee, S. O. Catt, L. Sielaff and E. Blasco, *Polym. Chem.*, 2025, **16**, 4571–4579.
6 A. Monmagnon, J. El Harfi, R. Demadrille and S. Rolere, *ACS Sustainable Chem. Eng.*, 2025, **13**, 21729–21739.
7 C. Vazquez-Martel, L. Florido Martins, E. Genthner, C. Almeida, A. Martel Quintana, M. Bastmeyer, J. L. Gómez Pinchetti and E. Blasco, *Adv. Mater.*, 2024, **36**, e2402786.
8 R. Sesia, M. Porcarello, M. Hakkarainen, S. Ferraris, S. Spriano and M. Sangermano, *Macromol. Chem. Phys.*, 2024, **226**, 2400181.
9 J. Stouten, G. H. M. Schnelting, J. Hul, N. Sijstermans, K. Janssen, T. Darikwa, C. Ye, K. Loos, V. S. D. Voet and K. V. Bernaerts, *ACS Appl. Mater. Interfaces*, 2023, **15**, 27110–27119.
10 V. Kirianchuk, Z. Demchuk, Y. Polunin, A. Kohut, S. Voronov and A. Voronov, *Molecules*, 2022, **27**, 932.
11 E. M. Maines, M. K. Porwal, C. J. Ellison and T. M. Reineke, *Green Chem.*, 2021, **23**, 6863–6897.
12 H. Fouilloux and C. M. Thomas, *Macromol. Rapid Commun.*, 2021, **42**, e2000530.
13 R. M. Cywar, N. A. Rorrer, C. B. Hoyt, G. T. Beckham and E. Y. X. Chen, *Nat. Rev. Mater.*, 2021, **7**, 83–103.
14 S. Shan, D. Mai, Y. Lin and A. Zhang, *ACS Appl. Polym. Mater.*, 2021, **3**, 5115–5124.
15 V. S. D. Voet, J. Guit and K. Loos, *Macromol. Rapid Commun.*, 2020, **42**, 2000475.
16 N. Bensabeh, A. Moreno, A. Roig, O. R. Monaghan, J. C. Ronda, V. Cadiz, M. Galia, S. M. Howdle, G. Lligadas and V. Percec, *Biomacromolecules*, 2019, **20**, 2135–2147.
17 Y. Xia and R. C. Larock, *Green Chem.*, 2010, **12**, 1893–1909.
18 G. Lligadas, J. C. Ronda, M. Galià and V. Cádiz, *Mater. Today*, 2013, **16**, 337–343.

19 J. A. Adeyera, J. A. Conti Silva, K. Kardel and R. L. Quirino, *ACS Omega*, 2025, **10**, 51322–51334.
20 C. Bodhak, T. Patel, P. Sahu and R. K. Gupta, *ACS Appl. Polym. Mater.*, 2024, **6**, 12886–12896.
21 M. Bergoglio, Z. Najmi, A. Cochis, M. Miola, E. Vernè and M. Sangermano, *Polymers*, 2023, **15**, 4089.
22 F. Zhao, W.-Q. Lian, Y.-D. Li, Y. Weng and J.-B. Zeng, *Ind. Crops Prod.*, 2022, **187**, 11091–11099.
23 C. Noè, A. Cosola, C. Tonda-Turo, R. Sesana, C. Delprete, A. Chiappone, M. Hakkarainen and M. Sangermano, *Polymer*, 2022, **247**, 124779.
24 A. Barkane, O. Platnieks, M. Jurinovs and S. Gaidukovs, *Polym. Degrad. Stab.*, 2020, **181**, 109347.
25 P. Zhang, J. Xin and J. Zhang, *ACS Sustainable Chem. Eng.*, 2013, **2**, 181–187.
26 R. Saraswat, Shagun, A. Dhir, A. S. S. Balan, S. Powar and M. Doddamani, *RSC Sustainability*, 2024, **2**, 1708–1737.
27 J. Thomas and R. Patil, *Ind. Eng. Chem. Res.*, 2023, **62**, 1725–1735.
28 C. Gaglieri, R. T. Alarcon, A. de Moura and G. Bannach, *Curr. Res. Green Sustainable Chem.*, 2022, **5**, 100343.
29 C. Zhang, T. F. Garrison, S. A. Madbouly and M. R. Kessler, *Prog. Polym. Sci.*, 2017, **71**, 91–143.
30 J. Guit, M. B. L. Tavares, J. Hul, C. Ye, K. Loos, J. Jager, R. Folkersma and V. S. D. Voet, *ACS Appl. Polym. Mater.*, 2020, **2**, 949–957.
31 Z. Dong, H. Cui, H. Zhang, F. Wang, X. Zhan, F. Mayer, B. Nestler, M. Wegener and P. A. Levkin, *Nat. Commun.*, 2021, **12**, 247.
32 C. Vazquez-Martel, L. Becker, W. V. Liebig, P. Elsner and E. Blasco, *ACS Sustainable Chem. Eng.*, 2021, **9**, 16840–16848.
33 M.-Y. Liu, G.-M. Li, P.-Y. Wang, W.-Y. Ying, Y. Yang, C.-Y. Tang, Y.-Y. Li and S.-P. Chen, *J. Polym. Res.*, 2024, **31**, 177.
34 B. Wu, A. Sufi, R. Ghosh Biswas, A. Hisatsune, V. Moxley-Paquette, P. Ning, R. Soong, A. P. Dicks and A. J. Simpson, *ACS Sustainable Chem. Eng.*, 2019, **8**, 1171–1177.
35 P. Rade, S. Swami, V. Pawane, R. Hawaldar, V. Giramkar, S. Joseph and B. Kale, *Polym. Eng. Sci.*, 2024, **64**, 2202–2213.
36 J. R. Tumbleston, D. Shirvanyants, N. Ermoshkin, R. Janusziewicz, A. R. Johnson, D. Kelly, K. Chen, R. Pinschmidt, J. P. Rolland, A. Ermoshkin, E. T. Samulski and J. M. DeSimone, *Science*, 2015, **347**, 1349–1352.
37 D. M. Shah, J. Morris, T. A. Plaisted, A. V. Amirkhizi and C. J. Hansen, *Addit. Manuf.*, 2021, **37**, 101736.
38 A. Khecho, M. M. T. Rahman, D. Reddy, A. El-Ghannam and E. B. Joyee, *Composites, Part B*, 2025, **296**, 112236.
39 D. A. Komissarenko, P. S. Sokolov, A. D. Evstigneeva, I. A. Shmeleva and A. E. Dosovitsky, *Materials*, 2018, **11**, 2350.
40 R. J. Mondschein, A. Kanitkar, C. B. Williams, S. S. Verbridge and T. E. Long, *Biomaterials*, 2017, **140**, 170–188.
41 Y. Liu, M.-Y. Liu, X.-G. Fan, L. Wang, J.-Y. Liang, X.-Y. Jin, R.-J. Che, W.-Y. Ying and S.-P. Chen, *ACS Sustainable Chem. Eng.*, 2022, **10**, 16344–16358.
42 C. Kolb, N. Lindemann, H. Wolter and G. Sextl, *J. Appl. Polym. Sci.*, 2020, **138**, 49691.
43 S. Krishnamoorthy, S. Wadnap, B. Noorani, H. Xu and C. Xu, *Eur. Polym. J.*, 2020, **124**, 109487.
44 V. Sereikaite, A. Navaruckiene, J. Jaras, E. Skliutas, D. Ladika, D. Gray, M. Malinauskas, V. Talacka and J. Ostrauskaite, *Polymers*, 2022, **14**, 5361.
45 J.-T. Miao, S. Peng, M. Ge, Y. Li, J. Zhong, Z. Weng, L. Wu and L. Zheng, *ACS Sustainable Chem. Eng.*, 2020, **8**, 9415–9424.
46 S. Rengasamy and V. Mannari, *Prog. Org. Coat.*, 2013, **76**, 78–85.
47 S. Briede, O. Platnieks, A. Barkane, I. Sivacovs, A. Leitans, J. Lungevics and S. Gaidukovs, *Coatings*, 2023, **13**, 657.
48 M. Danish, P. Vijay Anirudh, C. Karunakaran, V. Rajamohan, A. T. Mathew, K. Koziol, V. K. Thakur, C. Kannan and A. S. S. Balan, *J. Appl. Polym. Sci.*, 2021, **138**, 50903.